Nanoscale

FEATURE ARTICLE

View Article Online
View Journal | View Issue

Cite this: *Nanoscale*, 2016, **8**, 104

pH-Sensitive self-assembling nanoparticles for tumor near-infrared fluorescence imaging and chemo–photodynamic combination therapy†

Wenxiu Hou,[a,b] Xin Zhao,[a] Xiaoqing Qian,[a,b] Fei Pan,[a] Chunlei Zhang,[a] Yuming Yang,*[a] Jesús Martínez de la Fuente[a,c] and Daxiang Cui*[a]

The development of visual tumor theranostic nanoparticles has become a great challenge. In this study, D-α-tocopheryl polyethylene glycol 1000 succinate (TPGS) was conjugated to acid-sensitive *cis*-aconitic anhydride-modified doxorubicin (CAD) to obtain pH-sensitive anti-tumor prodrug nanoparticles (TCAD NPs) *via* self-assembling. Subsequently, the photosensitizer chlorin e6 (Ce6) was loaded into the resulting prodrug nanoparticles to prepare a novel tumor near-infrared fluorescence imaging and chemo–photodynamic combination therapy system (TCAD@Ce6 NPs). An accelerated release of doxorubicin (DOX) and chlorin e6 (Ce6) from the TCAD@Ce6 NPs could be achieved due to the hydrolysis of the acid-sensitive amide linker under mild acidic conditions (pH = 5.5). An *in vitro* experiment showed that A549 lung cancer cells exhibited a significantly higher uptake of DOX and Ce6 by using our delivery system than the free form of DOX and Ce6. An *in vivo* experiment showed that TCAD@Ce6 NPs displayed better tumor targeting gathering through the enhanced permeability and retention (EPR) effect than free Ce6, thus improving fluorescence imaging. Moreover, the chemo–photodynamic combination therapy of TCAD@Ce6 NPs combined with near-infrared laser irradiation was confirmed to be capable of inducing high apoptosis and necrosis of tumor cells (A549) *in vitro* and to display a significantly higher tumor growth suppression in the A549 lung cancer-bearing mice model. Furthermore, compared with exclusive chemotreatment (DOX) or photodynamic treatment (Ce6), our system showed enhanced therapeutic effects both *in vitro* and *in vivo*. In conclusion, the high performance TCAD@Ce6 NPs can be used as a promising NIR fluorescence imaging and highly effective chemo–photodynamic system for theranostics of lung cancer, *etc.* in the near future.

Received 3rd October 2015,
Accepted 9th November 2015

DOI: 10.1039/c5nr06842h

www.rsc.org/nanoscale

Introduction

Lung cancer has become the no. 1 leading cause of death worldwide and the number of lung cancer patients is rising remarkably.[1] Current cancer therapeutic methods mainly include surgery, chemotherapy, radiotherapy and immunotherapy. Doxorubicin (DOX) is a highly effective chemotherapeutic drug used to treat a wide variety of tumors such as breast cancer, prostate cancer, brain cancer, lung cancer, *etc.*[2,3] Furthermore, DOX with anthracycline can interact with DNA to block gene replication and transcription.[4,5] However, free DOX is not widely used in chemotherapy due to its short half-life and cytotoxicity to important organs such as the heart, kidney, *etc.*[6,7] Therefore, it is very necessary to develop novel efficient delivery formulations of DOX to improve its clinical efficacy and safety. To date, numerous DOX delivery systems have been developed to improve the antitumor therapeutic efficacy of DOX, including nanoparticles,[8] intelligent micelles,[4] liposomes,[9] and dendrimers.[10] Nonetheless, chemotherapy is accompanied by several side effects derived from its toxicity and terrible pain, making this treatment far from ideal. Scientists have already taken advantage of the combined therapy to boost the therapeutic efficiency and simultaneously reduce the side effects of cancer chemotherapy.[11–14]

In recent years, photodynamic therapy (PDT), another effective cancer treatment method, has attracted broad attention.

[a]*Institute of Nano Biomedicine and Engineering, Key Laboratory for Thin Film and Microfabrication Technology of the Ministry of Education, Department of Instrument Science and Engineering, School of Electronic Information and Electrical Engineering, Shanghai Jiao Tong University, Shanghai 200240, P.R. China. E-mail: yumingyang@sjtu.edu.cn, dxcui@sjtu.edu.cn*
[b]*School of Biomedical Engineering, Shanghai Jiao Tong University, Shanghai 200240, P.R. China*
[c]*Instituto de Nanociencia de Aragón, Universidad de Zaragoza, Spain*
† Electronic supplementary information (ESI) available: Additional experimental results. See DOI: 10.1039/c5nr06842h

The principle of PDT treatment is that certain photosensitive compounds can produce highly reactive oxygen species (ROS) upon photoexcitation which irreversibly induce cell apoptosis or necrosis in the targeted tissue.[15] In addition, because these photosensitizers also emit fluorescence signals under light excitation, they can serve as a contrast agent for tumor fluorescence imaging.[16] Although PDT has been used to treat some tumors, the potential of photosensitizers to be widely applied to cancer therapy is still hampered by many limitations such as their water-insolubility and low tumor targeted accumulation.[17,18] To overcome these drawbacks of photosensitizers for PDT, various nanoparticle-based systems have been developed to enhance the tumor targeting and PDT efficacy of photosensitizers.[9,19,20] Moreover, based on the attractive tumor therapy properties of PDT, the combined treatment of photodynamic and chemotherapy may optimize cancer treatment and achieve enhanced antitumor efficiency. Chlorin e6 (Ce6) is one of those promising photosensitizers, and it has been approved as a tool for photodynamic diagnostics in clinical application by FDA.[21,22] Due to its high singlet oxygen quantum yield and absorption/emission wavelength in the NIR region it can induce necrosis of tumors by deeper tissue penetration, therefore Ce6 should be an excellent photosensitizer for PDT.[23–26]

In addition, TPGS is a water-soluble amphiphilic macromolecule derived from natural vitamin E, and it has been widely used as an effective emulsifier or solubilizer.[27–29] TPGS is characterized by its bulky nature, water-solubility, and large surface area that make it a good candidate to serve as a promising drug delivery system enhancing the solubility and bioavailability of anticancer drugs. Actually, since FDA approved its clinical application, as a safe drug delivery system, it is widely used in cancer therapy with a high chemotherapeutic efficacy and low toxic side effects.[30–32]

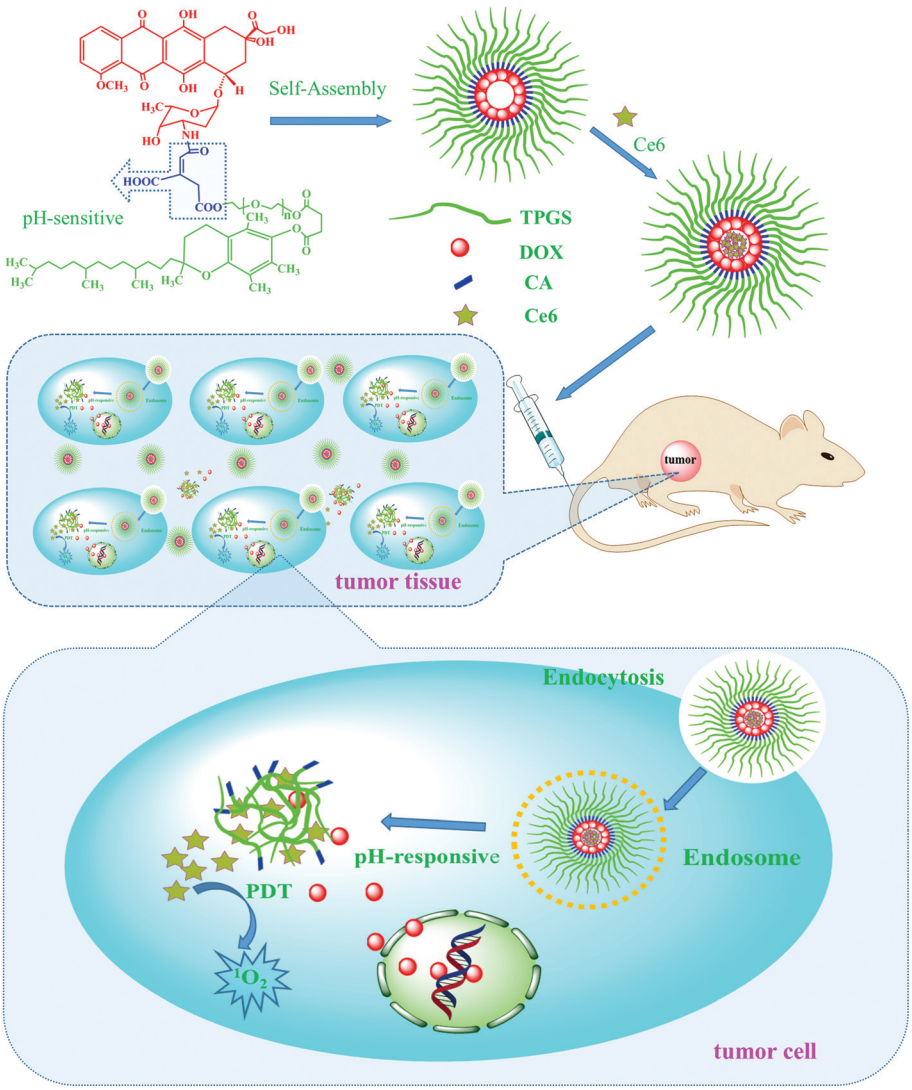

Scheme 1 Schematic illustration of the preparation of the TCAD@Ce6 NPs and their applications *in vitro* and *in vivo*. CA: *cis*-aconitic anhydride.

Therefore, in order to optimize the chemotherapeutic efficacy of doxorubicin (DOX) and improve the fluorescence diagnosis and PDT efficacy of photosensitizer chlorin e6 (Ce6), we firstly focus on developing D-α-tocopheryl polyethylene glycol 1000 succinate as the carrier of the hydrophobic chemotherapeutic agent doxorubicin (DOX) and the photosensitizer chlorin e6 (Ce6) for simultaneous tumor near-infrared fluorescence imaging and chemo–photodynamic combination therapy. Briefly, pH-sensitive *cis*-aconitic anhydride (CA)-modified DOX (CAD) was firstly synthesized, then the hydroxyl terminal group of TPGS was bonded with the carboxyl group of *cis*-aconitic anhydride (CA)-modified DOX to synthesize pH-responsive prodrug nanoparticles (TCAD NPs) *via* self-assembling in aqueous solution (Fig. S1† and Scheme 1). Subsequently, chlorin e6 (Ce6) was loaded into the resulting prodrug nanoparticles to prepare TCAD@Ce6 nanoparticles (TCAD@Ce6 NPs), with TPGS as the hydrophilic shell, and chlorin e6 and DOX as the hydrophobic core. Thanks to the characteristic lower pH value present in tumor tissues and also in some intracellular vesicles as endosomes and lysosomes,[5,33] the acid-sensitive amide linker present in our TCAD@Ce6 nanoparticles acts as "OFF/ON" switch. Under ideal circumstances, our theranostic nanoparticles would not leak DOX and would self-quench the fluorescence of Ce6 by π–π interactions in blood circulation. Due to the enhanced permeability and retention (EPR) effect, TCAD@Ce6 NPs could be gradually accumulated into the tumor location, where TCAD@Ce6 NPs could be activated to rapidly release DOX and Ce6 (Scheme 1) improving tumor NIR imaging, and enhancing chemo–photodynamic therapy.[19] In these studies the physicochemical properties, cellular uptake efficacy, *in vitro* phototoxicity, *in vivo* tumor targeting efficacy, and *in vivo* therapeutic efficacy of TCAD@Ce6 NPs were evaluated. The results showed that the developed acid-sensitive TCAD@Ce6 NPs displayed enhanced anti-tumor activity, specific tumor targeting and enhanced fluorescence imaging efficacy. Therefore, the exploited acid-sensitive TCAD@Ce6 NPs exhibit great potential in applications such as tumor NIR fluorescence imaging and simultaneous chemo–photodynamic therapy in the near future.

Experimental

Materials

Doxorubicin was obtained from Dalian Meilun Biotech Co., Ltd (Dalian, China). D-α-tocopheryl polyethylene glycol 1000 succinate (TPGS) was purchased from Ai Keda Chemical Technology Co., Ltd (Chengdu, China). *cis*-Aconitic anhydride (CA) was received from Meryer Chemical Technology Co., Ltd (Shanghai, China). *N*,*N*′-Dicyclohexylcarbodiimide (DCC), *N*-hydroxysuccinimide (NHS), triethylamine (TEA), anhydrous dimethyl sulfoxide (DMSO), and tetrahydrofuran (THF) were purchased from Aladdin Reagent Co., Ltd (Shanghai, China). 3-[4,5-Dimethylthiazol-2yl]-2,5-diphenyltetrazolium bromide (MTT) was obtained from Sigma Chemical Corporation (USA). Annexin V-FITC/PI Apoptosis Detection Kit was purchased from Yeasen Corporation (Shanghai, China). Hoechst 33342 and 2′,7′-dichlorofluorescein diacetate (DCFH-DA) were purchased from Invitrogen Corporation (Carlsbad, CA, USA). Chlorin e6 (Ce6) was obtained from Frontier Scientific (Utah, USA). All other chemicals were of reagent grade. Water was purified with a Milli-Q Plus 185 water purification system (Millipore, Bedford, MA).

Preparation of the TCAD nanoparticles

cis-Aconitic anhydride modified doxorubicin (DOX) was prepared as previously reported with some changes.[34] Doxorubicin hydrochloride (DOX·HCl) with twice the molar concentration of triethylamine (TEA) was dissolved in DMSO. The mixture was stirred overnight and light-protected at room temperature to obtain the doxorubicin (DOX) base. *cis*-Aconitic anhydride (50 mg) dissolved in 5 mL of dioxane was added dropwise to DOX (50 mg, previously dissolved in 5 mL of pyridine) under intensive stirring. The reaction mixture was stirred overnight at 4 °C protected from light. After that, the products were extracted five times with 10 mL chloroform and 10 mL of 5% sodium bicarbonate (aqueous solution). Then, the precipitate present in the aqueous phase was removed by centrifugation at 4 °C (10 000 rpm, 5 min). The pH of the supernatant was adjusted by adding hydrochloric acid (1 N) until the precipitate was separated out (pH about 2.5–3.0). Then, the solution was stirred for another 30 min to collect the precipitate by centrifugation at 4 °C (10 000 rpm, 10 min). The precipitate was washed with distilled water to remove the saline solution. The final product, referred to as "*cis*-aconitic anhydride-modified doxorubicin", was dried by lyophilisation. The yield of CAD was 50%.

Synthesis of TPGS–CAD conjugates. CAD (20 mg) was dissolved in 5 mL DMSO stirred for 30 min and then EDC·HCl (27.79 mg), DMAP (2.12 mg), and DCC (11.95 mg) were added to the CAD solution and incubated for about additional 3 h to activate the carboxyl of CAD. TPGS (39.8 mg) was dissolved in 2 mL DMSO, added dropwise to the solution and incubated for 24 h. Both steps were performed in the dark at 38 °C. The insoluble byproduct (dicyclohexylurea) was removed by filtration of the reaction mixture. The filtrate was separated by dialysis (MWCO 3500) against PBS (pH 8.0) for 1 day, and then against ultrapure water for 2 days. The final product referred to as the "TPGS–CAD conjugate (TCAD)" was dried by lyophilization. The yield of TCAD was 67%.

Preparation of TCAD nanoparticles. In brief, 5 mg TCAD was dissolved in 2 mL of tetrahydrofuran (THF), then 8 mL deionized water was added dropwise into the above solution. The reaction solution was stirred at room temperature for 30 min, whereafter the THF was removed by rotary evaporation and the residue was resuspended in deionized water, followed by filtering through a 0.45 μm pore-sized microporous membrane.

Preparation of TCAD@Ce6 nanoparticles

Chlorin e6 (Ce6) was loaded into TCAD using a simple dialysis method. Briefly, Ce6 (2 mg) dissolved in 1 ml of 1 : 1 (v/v) THF/DMSO was slowly added to TCAD (15 mg) dissolved in 6 mL of

distilled water. The mixed solution was thereafter sonicated for 30 min at 100 W. Then the solution was stirred at room temperature for 12 h under light-protection. The product was separated by dialysis (MWCO 3500) against 0.1 M $NaHCO_3$ for 12 h, and then against ultrapure water for 2 days. The Ce6 loading capacity was estimated by the ultraviolet absorbance at 660 nm (Fig. S2(B), ESI†) of Ce6.[35] The final product was filtered through a 0.45 μm pore-size microporous membrane.

The Entrapment Efficiency (EE) and Drug-Loading (DL) capacity were calculated using the following equations:

$$\mathrm{EE}(\%) = \text{weight of Ce6 in nanoparticles/weight of Ce6 fed initially} \times 100\%;$$

$$\mathrm{DL}(\%) = \text{weight of Ce6 in nanoparticles/weight of Ce6 in nanoparticles and weight of carriers} \times 100\%;$$

Characterization

The size and morphology of the TCAD NPs and TCAD@Ce6 NPs were characterized by TEM on a JEM-2100F (JEOL, Japan). The size and morphology of TCAD NPs were also measured by field emission scanning electron microscopy (FESEM: Zeiss). UV-Vis spectra were recorded with a Varian Cary 50 spectrophotometer (Varian Inc., Palo Alto, CA, USA). PL spectra were recorded on a Hitachi FL-4600 spectrofluorometer. DLS (dynamic light scattering) measurements were completed using a Nicomp 380 ZLS Zeta potential/Particle sizer (PSS Nicomp, Santa Barbara, CA, USA). ^{1}H NMR spectra were acquired using a Bruker Avance-III-HD 600 MHz NMR Spectrometer (Bruker BioSpin Corp., Billerica, MA, USA). Fourier transform infrared (FT-IR) spectra were recorded on a Bio-Rad WinIR Instrument using the potassium bromide method.

Critical aggregation concentration (CAC) measurement

Pyrene was used for the fluorescence probe to determine the CAC value of the TCAD NPs. 1 μL of pyrene acetone solution (6×10^{-4} mol L^{-1}) was added to 1 mL of TCAD aqueous solution with different concentrations. The mixture was sonicated for 30 min and then was incubated for extra 12 h in the dark at room temperature. The fluorescence intensity of the emission wavelengths (λ_{em}) of 384 nm (I_3) and 373 nm (I_1) of all samples was recorded on a Hitachi FL-4600 spectrofluorometer at 336 nm excitation wavelength and 5 nm slit width. The I_3/I_1 values of all samples were calculated and analyzed as a function of the logarithm of the nanoparticle concentration.

Measurement of *in vitro* DOX and Ce6 release

To evaluate the *in vitro* release profiles of DOX and Ce6 from TCAD@Ce6 NPs, 2 mL of TCAD@Ce6 NPs (0.5 mg mL^{-1}) was dissolved in PBS and subsequently transferred into a membrane tubing (MWCO 3500 Da). It was incubated in 80 mL PBS at pH 7.4 (a mimicking normal physiological condition), pH 6.5 (a tumor tissue acidic microenvironment) and pH 5.5 (an intracellular acidic microenvironment), with continuous shaking at 100 rpm at 37 °C, respectively. At predetermined time intervals, 1 mL of release medium was taken out, and an equal volume of fresh PBS was returned to the system. The accumulative amount of the released DOX and Ce6 was detected from UV-Vis spectra at 480 nm for DOX and at 660 nm for Ce6.

TCAD@Ce6 NPs (4 μg mL^{-1} of Ce6 equivalents) in DMEM medium with 10% FBS were incubated with or without A549 cells for different times at 37 °C to detect the fluorescence intensity changes of TCAD@Ce6 NPs in tumor cells. Near-infrared (NIR) fluorescence images were then recorded with a Bruker In-Vivo F PRO imaging system. Moreover, the fluorescence intensity changes of TCAD@Ce6 NPs were also measured by using PL spectra before and after their incubation at 37 °C in PBS (pH 5.5) for 24 h.

Cell culture

Human non-small cell lung cancer cells (A549 cells) were used for cell studies. A549 cells were incubated in DMEM medium with 10% FBS at 37 °C with 5% CO_2. Before experiments, the cells were pre-cultured until 75% confluence was reached.

In vitro cellular uptake and distribution of TCAD

For confocal microscopy experiments: A549 cells were plated onto coverglass in 24-well plates at a density of 2.0×10^4 cells per well and allowed to adhere for 24 h. Then, the culture medium was replaced with a fresh medium containing 4 μg mL^{-1} free Ce6, 5.86 μg mL^{-1} free DOX, TCAD NPs (5.86 μg mL^{-1} of DOX equivalents), or the TCAD@Ce6 NPs (4 μg mL^{-1} of Ce6 equivalents, 5.86 μg mL^{-1} of DOX equivalents). After 4 h and 12 h co-incubation, the cells were washed twice with PBS sufficiently and then fixed with 2.5% glutaraldehyde at 4 °C for 30 min. The nuclei of the cells were stained with Hoechst 33342 at room temperature for 15 min. Confocal fluorescence imaging studies were performed with a TCS SP8 confocal laser scanning microscope. Hoechst 33342 was excited using the blue diode 405 nm laser and the emission was recorded between 440 and 470 nm. Ce6 was excited at 633 nm and the emission was collected from 650 to 800 nm. DOX was excited at 488 nm and the emission was collected from 500 to 590 nm.

Flow cytometry (BD FACSCalibur) measurements to quantify the cellular uptake: A549 cells (1.0×10^5 cells per well in 6-well plates) were cultured in medium for 24 h, and co-incubated with free Ce6, free DOX, TCAD NPs or TCAD@Ce6 NPs (with the same concentrations of confocal fluorescence imaging studies) for 4 h and 12 h, respectively whereafter the cells were washed with PBS and then the cells were trypsinized and resuspended in 0.5 mL of PBS for flow cytometry measurements. The fluorescence signals of Ce6 and DOX were collected by using FL3-H and FL1-H channels, respectively.

Cell viability and apoptosis assay

Cellular ROS (reactive oxygen species) detection during irradiation. The intracellular ROS generation was monitored by staining all the cells with DCFH-DA. The A549 cells were incubated with PBS, free Ce6 (4 μg mL^{-1}) or TCAD@Ce6 NPs

(equivalent Ce6 4 μg mL^{-1}) in a six-well plate. After 24 h co-culture, the cells were further incubated with 20 μM DCFH-DA for 20 min and irradiated using a 633 nm He–Ne laser at a power of 50 mW cm^{-2} for 3 min or not. Subsequently, the fluorescence intensity of DCF inside the cells, which was proportional to the amount of ROS produced, was detected by flow cytometry.

In addition, the singlet oxygen sensor green (SOSG) reagent, which is highly selective for $^1O_2$, was employed to measure the $^1O_2$ generation of the TCAD@Ce6 NPs (equivalent Ce6 4 μg mL^{-1}) at different irradiation times at 633 nm (50 mW cm^{-2}) (excitation = 494 nm).

MTT assay. The dark toxicity and phototoxicity of free Ce6 and TCAD@Ce6 NPs were determined by the MTT assay of A549 cells. Briefly, the A549 cells were seeded in a 96-well plate at a density of 5×10^3 cells per well. After 24 h incubation, the cells were incubated with 100 μL fresh complete medium containing serial concentrations of free Ce6 (0.1–4 μg mL^{-1}) or TCAD@Ce6 NPs (equivalent Ce6 0.1–4 μg mL^{-1}) or PBS (control group). After incubation for 12 h at 37 °C in the dark, the cells were washed twice with fresh medium, one plate was kept in the dark to study dark toxicity, and the other plate was irradiated using a 633 nm helium–neon (He–Ne) laser at a power of 50 mW cm^{-2} for 1.5 min and 3 min, respectively. After extra 12 h of incubation in the dark, the dark toxicity and phototoxicity were evaluated by the MTT assay. The cell viability was calculated according to the equation: cell viability = (OD 570 nm of the experimental group/OD 570 nm of the control group) × 100% and the cell viability of the control group were denoted as 100%. According to the above protocol, the MTT assay was also carried out to evaluate the cytotoxicity of free DOX and TCAD NPs. The A549 cells were incubated with 100 μL fresh complete medium containing serial concentrations of free DOX (0.1–6 μg mL^{-1}) and TCAD NPs (equivalent DOX 0.1–6 μg mL^{-1}) for 24 h and 48 h, respectively, before executing the MTT assay.

Visually observation of the photodynamic therapeutic efficacy. The A549 cells were seeded onto a 24-well plate (1×10^4 cells per well), and then incubated for 24 h. The medium was replaced with a fresh medium containing TCAD@Ce6 NPs (equivalent Ce6 4 μg mL^{-1}), or the free Ce6 (4 μg mL^{-1}). After 12 h incubation in the dark, the A549 cells were changed to fresh culture medium, irradiated with or without an NIR laser (633 nm, 50 mW cm^2) for 3 min. After another 12 h incubation in the dark, the cells were washed with PBS and stained with Calcein-AM and PI. The live cells and dead cells were stained by using Calcein-AM and PI, respectively.

Apoptosis assay. The apoptotic and necrotic cell distributions were tested according to the manufacturer's instruction using the Annexin V-FITC/PI Apoptosis Detection Kit. The A549 cells were exposed to free Ce6 (4 μg mL^{-1}) or the TCAD@Ce6 NPs (equivalent Ce6 4 μg mL^{-1}) for 12 h. Then, the cells were washed twice with 1 × PBS and the medium was replaced with fresh complete culture medium, followed by irradiation with or without a 633 nm He–Ne laser at a power of 50 mW cm^{-2} for 3 min. Afterward, the cells were trypsinized, harvested, washed with 1 × PBS and resuspended in 190 μL of binding buffer. Finally, the cells were stained with 5 μL Annexin V and 5 μL PI in the dark at room temperature for 15 min. 300 μL of binding buffer was added to each sample before the cells were analyzed by using a BD FACSCalibur within 30 min. The data were analyzed by using FlowJo 7.6 software.

Tumor-targeting efficiency in tumor bearing mice

Female BALB/c-nude mice (4 weeks of age) were purchased from Shanghai Slac Laboratory Animal Co., Ltd (Shanghai, China). All animals received care in compliance with the Institutional Animal Care and Use Committee of Shanghai Jiao Tong University. The female nude mice were injected subcutaneously in the right flank region with 150 μL of cell suspension containing 4×10^6 A549 cells. The tumors were allowed to grow to reach a size of ~200 mm^3 before the biodistribution and imaging studies. Free Ce6 or TCAD@Ce6 NPs in saline (at a dosage of Ce6 4 mg kg^{-1} of total mouse body weight) were intravenously injected into the tumor-bearing mice. Fluorescence images were obtained at 2, 4, 12, and 24 h after injection by using a Bruker In-Vivo F PRO imaging system (Billerica, MA, USA) (excitation: 630/20 nm; emission: 700/30 nm; integration time: 10 s). The mice were sacrificed, and tumors and the major organs were collected at 24 h post-injection. The excised tumors and organs were imaged by using the Bruker In-Vivo F PRO imaging system with the same parameters as mentioned above. The average fluorescence intensity of tumors and other organs was quantified by using Bruker Molecular Imaging Software 7.1 Version.

Photodynamic therapeutic efficacy of TCAD@Ce6 NPs in tumor-bearing mice

In vivo chemotherapy, photodynamic and chemo–photodynamic treatments were performed using A549 tumor-bearing mice. When the tumor size reached ~100 mm^3, the mice were randomized into six groups of 3 animals per group. (1) PBS (150 μL) without a laser, (2) PBS (150 μL) with a laser, (3) free Ce6 (4 mg kg^{-1}) upon laser irradiation, (4) free DOX (5.86 mg kg^{-1}), (5) TCAD NPs (equivalent DOX 5.86 mg kg^{-1}) and (6) TCAD@Ce6 NPs (4 mg kg^{-1} of Ce6 equivalents, 5.86 mg kg^{-1} of DOX equivalents) with laser irradiation were injected into the tail vein, respectively. For the irradiated groups, a 633 nm He–Ne laser (50 mW cm^{-2}, 30 min) was used after 12 h of intravenous injection. The tumor images of A549 tumor-bearing mice were taken at the day before the tumors were exposed to the irradiation (0 day) and at 12 h (1 day), 4 days (4 day), 14 days (14 day) after irradiation, respectively. The tumor size and body weight were measured by using a caliper and an electronic balance every three days after treatment, respectively. Tumor volume = $a \times (b)^2 \times 1/2$, where a and b represent the maximum length and the minimal width of tumors, respectively. On day 18, the mice treated with TCAD@Ce6 NPs were sacrificed. The heart, liver, spleen, lung, and kidney were excised and further investigated after H&E staining to monitor the morphological features of each organ.

Results and discussion

Synthesis and characterization

To provide the prepared delivery system with acid-sensitive properties for tumor specific drug release, acid-sensitive *cis*-aconitic anhydride-modified DOX (CAD) was firstly prepared through the ring-opening reaction[4] (Fig. S1, ESI†). As shown in the ^{1}H NMR spectra (Fig. 1A – DOX), the peak at about 7.9 ppm belongs to the protons of the anthracene moiety of DOX. After *cis*-aconitic anhydride modification, additional signals at 6.1 and 6.4 ppm appeared, attributed to the protons (CH–COO–) of the *cis*-aconitic anhydride linkages in the structure of *cis*-DOX (Fig. 1A – CAD). Surface TPGS modification is demonstrated to further improve the cellular uptake and increase the half-life as well as the therapeutic effects of the drug.[36] Therefore, in this study we modified CAD with TPGS by the ester linkage (Fig. S1, ESI†). ^{1}H NMR spectra of TPGS and TCAD displayed an intense signal at around 2.0 ppm, attributed to the protons of succinyl methylene (Fig. 1B). Also, the characteristic peak of TPGS at 3.5 ppm belonging to the methylene protons of the mPEG part can be observed in both spectra of TPGS and TCAD (Fig. 1B). Because of the relatively small molecular weight of CAD, we could only see the much weaker intensity of CAD characteristic proton signals at around 8.0, 13.2, and 14.0 ppm (Fig. 1B, insert) compared with that of TPGS. FT-IR spectra were further used to confirm the structure of these formed compounds as shown in Fig. 1C. The signals that appeared at around 1548 cm^{-1} (amide II) in CAD were assigned to the characteristic signals of the formed amide bond. After the TPGS modification, the new absorption bands at 1111 cm^{-1} were attributed to the stretching modes of –CH_2–O–CH_2– of the TPGS, while the typical absorption bands at 3440 and 1633 cm^{-1} were associated with the stretch of the phenolic hydroxyl group and amide I of CAD. Moreover, the small peaks at 1695 and 1584 cm^{-1} indicated the formation of the ester group between TPGS and CAD (Fig. 1D). The TCAD was also characterized by ultraviolet-visible spectrophotometry (UV-Vis) (Fig. S2(A), ESI†). All of the above experiments confirmed the successful synthesis of TCAD. In water, the amphiphilicity character of the TCAD allows it to self-assemble into nanoparticles, with insoluble DOX as the hydrophobic core and TPGS as the hydrophilic shell. To perform tumor targeting fluorescence imaging and chemo–photodynamic combination therapy, chlorin e6 (Ce6) was loaded into the TCAD NPs to form the TCAD@Ce6 NPs *via* the self-assembly process. The loading efficacy, encapsulation efficiency and hydrodynamic diameter were altered with the change of *D*/*P* ratios (Table 1). To obtain high Ce6 loading ratios and reduce the waste of the Ce6, the *D*/*P* ratio of 20% was selected for further studies. The loading efficacy determined by UV-Vis spectroscopy was about 14.89%. The absorbance spectra of TCAD NPs, free Ce6 and TCAD@Ce6 NPs were measured by UV-Vis spectroscopy. TCAD@Ce6 NPs have a characteristic absorption peak of DOX at 480 nm and a bathochromic absorption peak of Ce6 at 659 nm (Fig. S2(B), ESI†). The bathochromic shift of the absorption peak of Ce6 may respond to the changes of the Ce6

Table 1 Characteristics of TCAD@Ce6 NPs after Ce6 loading

D/*P* ratio[a]	EE%	DL (%)	Diameter[b] (nm)
1 : 10	98.50%	8.96%	157.20 ± 3.1
1 : 20	85.25%	14.89%	160.00 ± 1.6

[a] *D*/*P* ratio = weight of Ce6/weight of TCAD. [b] Measured using dynamic light scattering (DLS), data represent mean ± SD, n = 3.

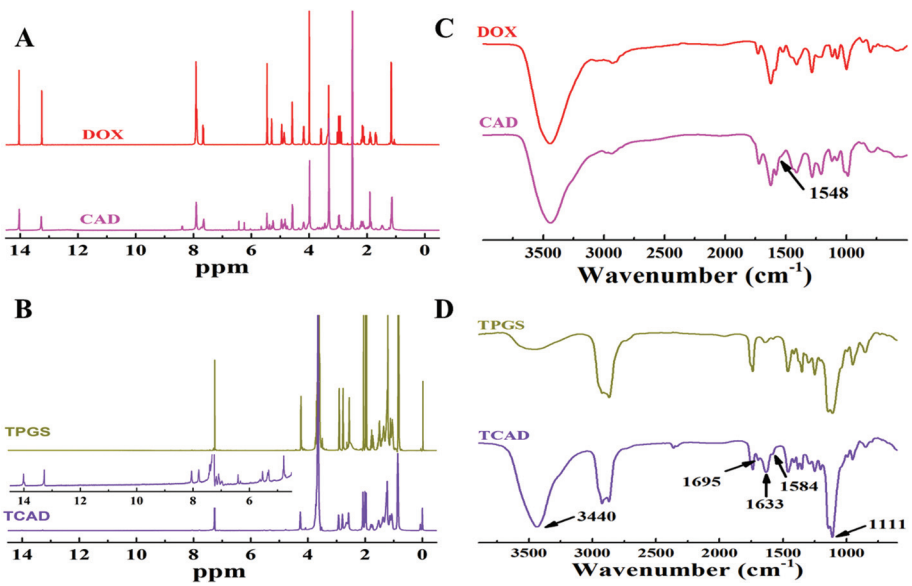

Fig. 1 ^{1}H NMR and FT-IR spectra of DOX (DMSO-d_6), CAD (DMSO-d_6), TPGS ($CDCl_3$), and TCAD ($CDCl_3$).

environment.[37] As a result, the Ce6 was successfully encapsulated into the TCAD NPs.

The hydrodynamic diameter of TCAD NPs (196.0 nm) and TCAD@Ce6 NPs (160.0 nm) in the range of 50–200 nm (Fig. S3 (A), ESI† and 2A, insert) indicated that TCAD NPs and TCAD@Ce6 NPs may preferentially distribute into the tumor by the enhanced permeability and retention (EPR) effect.[38,39] The morphology of the dried TCAD NPs and TCAD@Ce6 NPs was evaluated by transmission electron microscopy (TEM). The TEM image results proved that the TCAD NPs and TCAD@Ce6 NPs were almost spherical and uniform with good monodispersity (Fig. 2A and S2(B), ESI†). Moreover, the scanning electron microscopy (SEM) imaging of TCAD NPs showed a similar result to TEM (Fig. S3(C), ESI†). The size of TCAD@Ce6 NPs was smaller than TCAD NPs that may be owing to the addition of Ce6, which increases the hydrophobic interaction during the self-assembly process. More importantly, the results of the hydrodynamic diameter measured at fixed time points for a month indicated that the sizes of TCAD NPs and TCAD@Ce6 NPs fluctuate in a small scope, suggesting that both TCAD NPs and TCAD@Ce6 NPs are stable and can be stored in water for relatively long periods of time without sedimentation or aggregation (Fig. 2B). The critical aggregation concentrations (CACs) of TCAD NPs were determined by using pyrene as the fluorescent probe.[40] In detail, the CACs of micelles were related to the emission intensity ratio of the third and first bands (I_3/I_1) in the fluorescence spectrum of pyrene. The value of CAC was assessed from the first inflection point in the curve of the absorption intensity ratio of I_3/I_1 *versus* the logarithm of concentration.[41] The CAC value of TCAD NPs was calculated to be 23.4 μg mL^{-1} approximately (Fig. S4, ESI†).

In vitro DOX and Ce6 release

To demonstrate the acid-sensitivity of TCAD@Ce6 NPs, the *in vitro* DOX and Ce6 release behavior of TCAD@Ce6 NPs was measured by dialysis in PBS at pH 7.4, 6.5, and 5.5 at 37 °C, respectively. The results of cumulative release curves revealed DOX and Ce6 without significant burst release from TCAD@Ce6 NPs in PBS (pH 7.4), suggesting a good stability of TCAD@Ce6 NPs under normal physiological tissue conditions (Fig. 2C). Nevertheless, at mild acidic environmental pH 6.5 or even 5.5, which simulated the tumor tissular and intracellular microenvironment, respectively, the cumulative release of DOX and Ce6 was accelerated dramatically. When incubated with PBS (pH = 5.5), the cumulative release of DOX and Ce6 from the TCAD@Ce6 NPs was higher than that observed when incubated with PBS (pH = 6.5). On this basis, the TCAD@Ce6 NPs will release more of their drug cargo in the endo/lysosomal vesicles (pH 5.5) than in the solid tumor extracellular environment (pH 6.5). Moreover, most of the TCAD@Ce6 NPs may be taken up by the tumor cells before releasing their drug cargo. In this case, even if some of the drug cargo were released in the solid tumor extracellular environment they may enter the tumor cells by passive diffusion, which may have little influence on cellular uptake and therapeutic efficacy.[42,43] All the results may be attributed to the expedited hydrolysis of

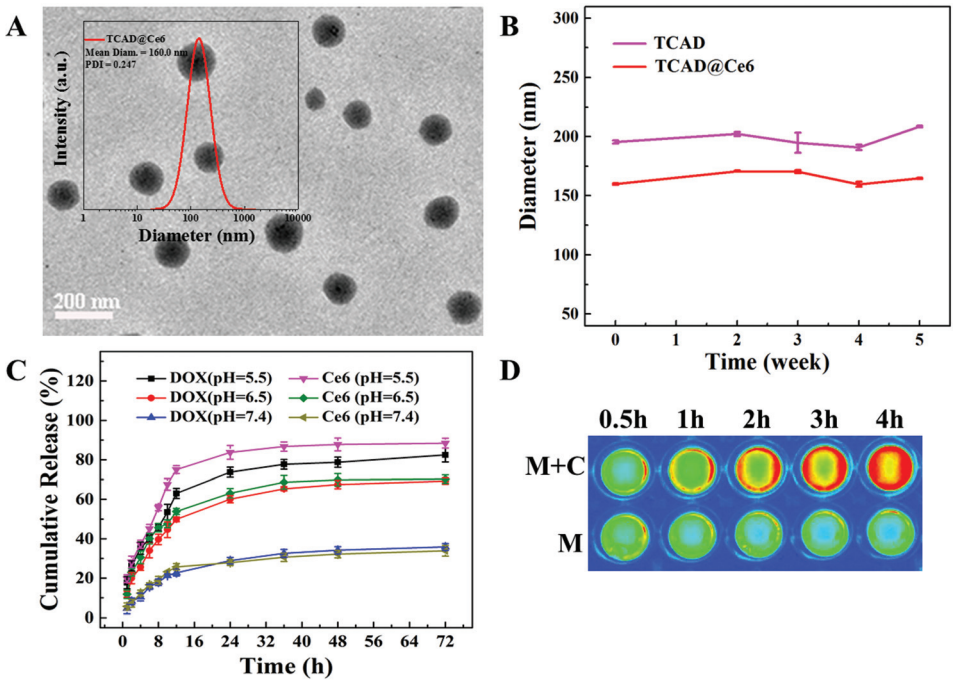

Fig. 2 Characterization of the nanoprobes. (A) Morphology of TCAD@Ce6 NPs observed by TEM and size distribution measured by DLS; (B) colloid stability test of TCAD and TCAD@Ce6 NPs in water; (C) cumulative release DOX and Ce6 from TCAD@Ce6 NPs at different pH; (D) the NIR image of TCAD@Ce6 NPs in culture medium (10% FBS) without cells (M) or co-incubated with A549 cells (M + C) for different times.

the acid-sensitive linker in an acidic environment. This acid-sensitive release of TCAD@Ce6 NPs makes them an interesting tool for clinical tumor chemo–photodynamic combination therapy that may minimize the damage of healthy tissues and maximize the therapeutic efficacy. The Ce6 was wrapped into the interior of TCAD@Ce6 NPs, which might cause the aggregation of Ce6 by π–π and hydrophobic interactions, resulting in a dramatic reduction of NIR fluorescence by self-quenching. That is, the recovery of NIR fluorescence of Ce6 from TCAD@Ce6 NPs can be correlated with the release of Ce6. To estimate the intracellular NIR fluorescence recovery of Ce6 in TCAD@Ce6 NPs, the NIR fluorescence images of TCAD@Ce6 NPs after co-incubation with or without A549 cells at different time points were analysed (Fig. 2D). In the absence of A549 cells, the fluorescence changed little in the medium over time. Noteworthily, the fluorescence intensity increased dramatically with the extending of the incubation time in the presence of A549 cells, suggesting that the Ce6 was gradually released from TCAD@Ce6 NPs inside the cell, resulting in the fluorescence recovery of Ce6. Moreover, the fluorescence of Ce6 in the TCAD@Ce6 NPs was dramatically lower than free Ce6 due to the self-quenching effect before being treated with mild acidic PBS (pH = 5.5). However, after 24 h incubation in mild acidic PBS (pH = 5.5), an obvious increase of the fluorescence intensity of Ce6 was detected (Fig. S5, ESI†). Therefore, we came to a conclusion that the acid-sensitive TCAD@Ce6 NPs would self-quench the phototoxicity in blood circulation to weaken the side effects and recover phototoxicity in the target tumor acid microenvironment.

Cellular uptake and intracellular distribution

The cellular uptake behavior of TCAD and TCAD@Ce6 nanoparticles was evaluated by confocal laser scanning microscopy (CLSM) and flow cytometry (FCM) toward A549 cells. Flow cytometry analysis after 4 h incubation (Fig. 3A and B) indicated that about 21.5% of A549 cells displayed a fluorescence signal from DOX in TCAD NPs, which is higher than that detected in free DOX (about 15.5%). However, after 12 hours incubation, the same analysis revealed that the ratio of A549 cells with the fluorescence signal of DOX when exposed to TCAD NPs was

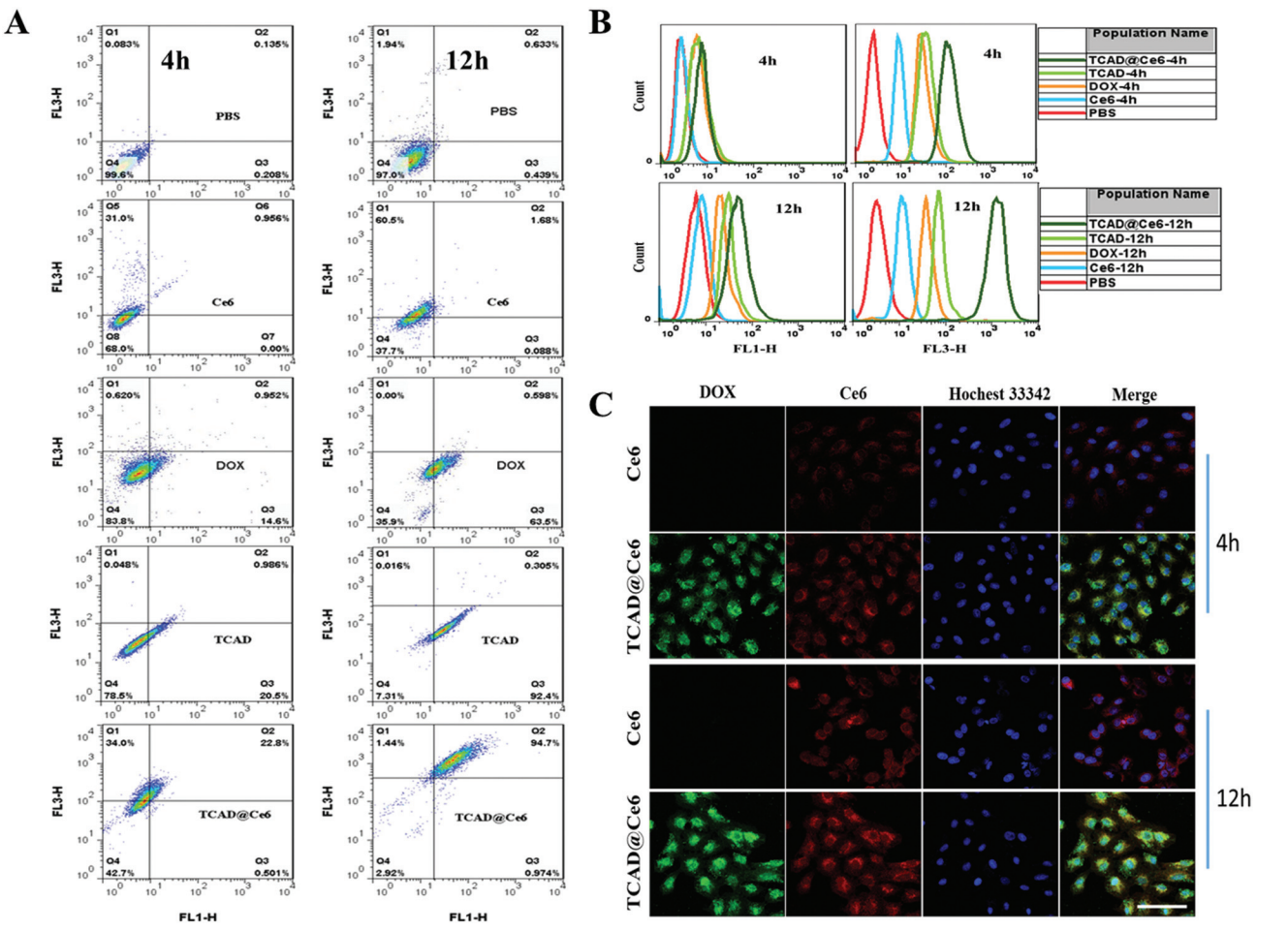

Fig. 3 Cellular uptake efficacy and localization. Flow cytometry separate analysis (A) and integral analysis (B) of cellular uptake of free Ce6, free DOX, TCAD and TCAD@Ce6 NPs for 4 h and 12 h, respectively; (C) confocal images of A549 cells exposed to free Ce6 or TCAD@Ce6 NPs for 4 h and 12 h, respectively. Scale bar, 100 μm.

increased to about 92.7%, which was higher than that of free DOX (about 64.1%). Meanwhile, the fluorescence signal intensity of DOX from TCAD NPs was similar to that of TCAD@Ce6 NPs in A549 cells with prolonged incubation time. Predictably, the cells co-cultured with TCAD@Ce6 for 4 h or 12 h exhibited significantly higher ratios of Ce6 fluorescence signal when compared to those incubated with free Ce6. It demonstrated that TCAD@Ce6 NPs would enhance the cellular uptake capability of Ce6 and DOX in A549 cells, compared with free Ce6 and free DOX. Overall, these phenomena may be due to the efficient endocytosis and rapid intracellular DOX and Ce6 release, which were induced by the intracellular acidic microenvironment-triggered hydrolysis of the amide linker in TCAD and TCAD@Ce6.[44]

DOX is a well known and widely used anticancer drug that shows the anti-cancer effect by damaging the DNA structure in nuclei.[45] Whereas Ce6, a common photosensitizer, tends to locate in the cytoplasm.[46] Next, TCAD NPs and TCAD@Ce6 NPs were incubated with A549 cells for 4 h and 12 h, respectively. Confocal microscopy images were utilized to visually show the cellular internalization and the intracellular release of DOX and Ce6. As shown in Fig. 3C, the green fluorescence and red fluorescence were used to localize the DOX and Ce6, respectively. Hoechst 33342 was used to stain the nuclei (blue). For free DOX, after being incubated with A549 cells for 4 h, very slight green fluorescence was detected, suggesting that free DOX entered the cells at low quantities. When incubation times were prolonged to 12 h, the green fluorescence of free DOX was spread all over the cells and the intensity of green fluorescence was enhanced (Fig. S6, ESI†). In contrast, in the case of TCAD NPs and TCAD@Ce6 NPs, DOX was observed to be highly accumulated in nuclei compared with free DOX, when incubated with A549 cells for 4 h (Fig. S6† and 3C). Meanwhile, a significant increase of the green fluorescence intensity of DOX in nuclei was detected, after TCAD NPs and TCAD@Ce6 NPs were incubated with A549 cells for 12 h. These observations demonstrated that TCAD NPs may be an attractive way to help DOX circumvent the multidrug resistance, enter into the cytoplasm and then diffuse into the nucleus. Additionally, the red fluorescence intensity of Ce6 in the cytoplasm from the TCAD@Ce6 NPs was higher than that of free Ce6, and increased remarkably with the extension of incubation time. In a word, the confocal microscopy images obtained are consistent with the results obtained by flow cytometry. The enhanced cell uptake of TCAD NPs and TCAD@Ce6 NPs may take advantage of endocytosis efficiently rather than passive diffusion through the cell membrane of free DOX and free Ce6.[47]

In vitro cellular toxicity

MTT assay was executed to detect the *in vitro* cellular proliferation inhibition of free DOX, and TCAD NPs against A549 cells. As shown in Fig. 4A, TCAD NPs exhibited more notable antiproliferation efficacy on A549 cells *in vitro* than that of equivalent free DOX, after 24 h or 48 h co-incubation. The trends became more significant with the increasing incubation time. The result was also verified by the apoptosis assay (Fig. 4B). These may take advantage of the cellular uptake enhancement of TCAD NPs and the quick release of DOX in the acidic intracellular microenvironment as demonstrated above.

Singlet oxygen would induce the damage of cellular constituents and subsequent cell death, which can denote the phototoxicity of nanoparticles.[20] The extracellular singlet oxygen production was detected by a singlet oxygen sensor green (SOSG) reagent. TCAD@Ce6 NPs exhibited the increased singlet oxygen generation capability along with prolongation of irradiation time (Fig. S7, ESI†). Moreover, the DCFH-DA staining method was employed to examine the intracellular singlet oxygen production for actual research on the phototoxicity of intracellular nanoparticles. As expected, detected by the flow cytometry assay, the TCAD@Ce6 NPs caused the most remarkable singlet oxygen production under irradiation compared with free Ce6 under irradiation and TCAD@Ce6 NPs without irradiation (Fig. S8, ESI†). Subsequently, the cytotoxic efficacy and the efficiency of chemo–photodynamic combination therapy of TCAD@Ce6 NPs to A549 cells with or without laser irradiation was further quantified by MTT assay and apoptosis assay. As shown in Fig. 4C, compared to treatment with free Ce6/laser, a significantly decreased survival ratio of A549 cells was detected when treated with TCAD@Ce6 NP/laser. In addition, after 24 h incubation, the survival ratio of A549 cells was 71.2% and 66.44% when treated with free Ce6 (4.0 μg mL^{-1}) upon laser irradiation for 3 min (Fig. 4C) and TCAD NPs (equivalent DOX 6.0 μg mL^{-1}) (Fig. 4A), respectively, while the cell survival ratio of A549 cells suddenly decreased to 15.73% when exposed to TCAD@Ce6 NPs (equivalent Ce6 4.0 μg mL^{-1} and equivalent DOX 5.86 μg mL^{-1}) plus laser irradiation for 3 min (Fig. 4C). That is, with the same concentrations of Ce6 plus laser irradiation or DOX, the TCAD@Ce6 NPs would lead to the mortality rate as high as about 2.9 times that treated with the free Ce6, and about 2.5 times higher than that treated with TCAD NPs. All the results indicated that the combination therapy resulted in a more striking tumor treatment effect than chemo or photodynamic treatment alone.

The flow cytometry assay reconfirmed that minimal apoptosis and necrosis of A549 cells (mortality ratio <11%) were induced by free Ce6 in the dark or cells with only laser exposure. Meanwhile, the ratio of apoptosis and necrosis was increased to 80% when the cells were exposed to TCAD@Ce6 NPs plus laser irradiation, while a slight increase in cell apoptosis was detected when treated with free Ce6 plus laser irradiation (Fig. 4D). Furthermore, the cell was stained with Calcein-AM and PI to visually detect the photodamage, when cultured with free Ce6 and TCAD@Ce6 NPs with or without a laser. The red fluorescence of PI and the green fluorescence of Calcein-AM were on the behalf of dead and live cells, respectively. As anticipated, after 3 min of irradiation, there was weak red fluorescence emitted from the cells treated with free Ce6, suggesting that little cells were photodamaged (Fig. 4E). The low cellular uptake and the little intracellular singlet oxygen

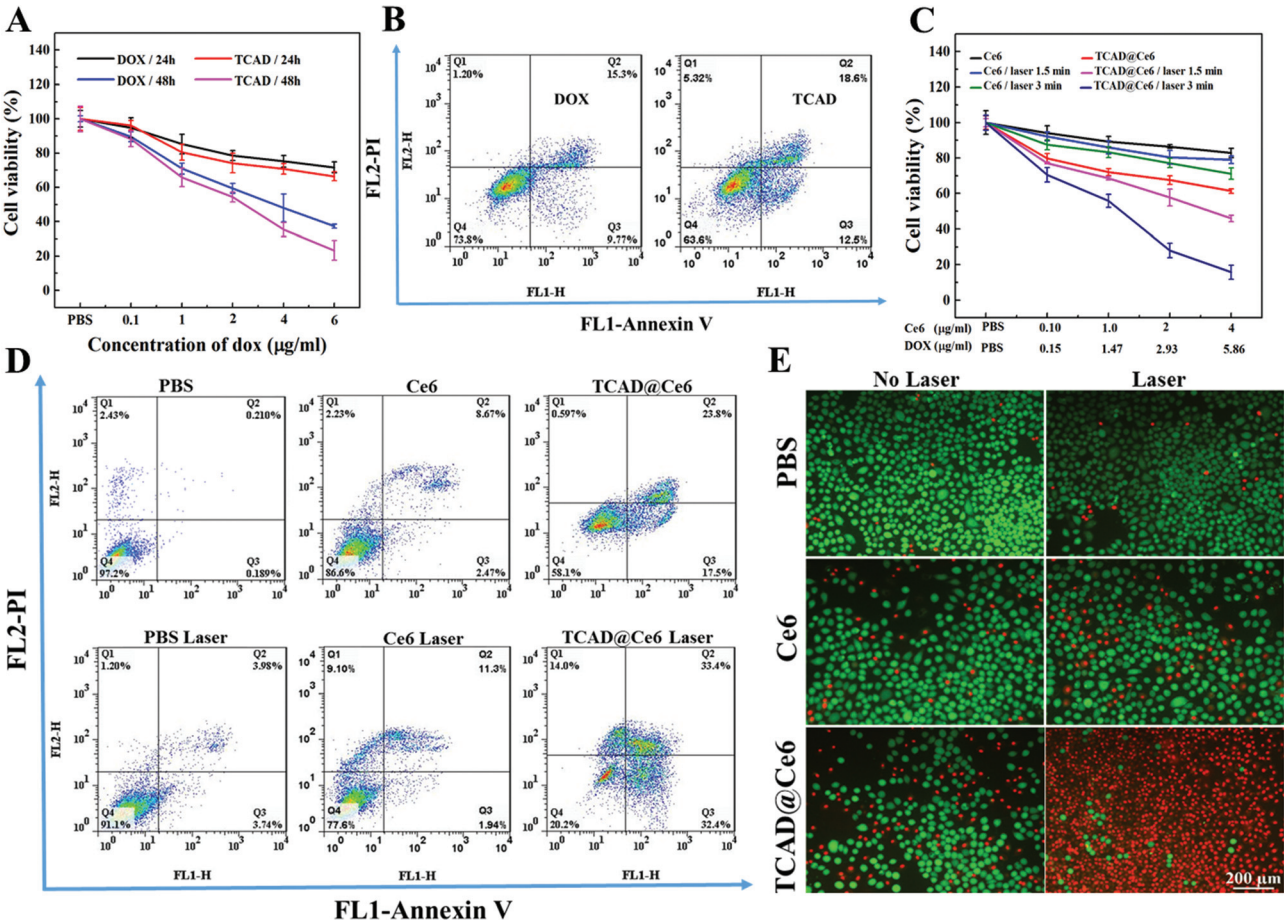

Fig. 4 *In vitro* cellular toxicity. MTT assay quantitative evaluation (A) and flow cytometry analysis (B) of cell survival for A549 cells treated with free DOX and TCAD NPs for 24 h and 48 h, respectively; dark toxicity and photocytotoxicity of free Ce6 and TCAD@Ce6 NPs towards A549 cells for 24 h, analyzed by the MTT assay (C) and flow cytometry (D), respectively; (E) detection of photodamage by fluorescence microscopy using fluorescent probes (double-staining with calcein PI and calcein-M). Dead cells: red fluorescence of PI, live cells: green fluorescence of calcein-AM. The data are shown as mean ± SD (n = 3).

production may be the likely reason. Nevertheless, the TCAD@Ce6 NP treated cells showed striking red fluorescence signals with laser irradiation. That is, the phototoxicity of TCAD@Ce6 NPs is higher than free Ce6 upon the NIR laser irradiation. The experimental results of the singlet oxygen detection test, MTT assay, apoptosis assay and Calcein-AM and PI staining assay were consistent, revealing that TCAD@Ce6 NPs may be a promising way for DOX delivery and PDT treatment.

Tumor-targeting evaluation of the TCAD@Ce6

The intrinsic NIR fluorescence of Ce6 allows the detection of the tumor targeting and *in vivo* distribution of TCAD@Ce6 NPs in A549 tumor-bearing nude mice by the NIR imaging approach. The Ce6 and TCAD@Ce6 NPs were tail vein injected into the A549 tumor-bearing nude mice to monitor their time dependent distribution *in vivo*. As shown in Fig. 5A, free Ce6 as a kind of small dye molecule, in the absence of tumor targeting, mainly accumulated in the liver and was rapidly catabolized from mice, whereas the TCAD@Ce6 NPs exhibited relatively high tumor targeting efficiency and relatively long tumor retention time. That is TCAD@Ce6 NPs for PDT would prolong the phototoxicity duration and enhance the tumor accumulation of Ce6. More importantly, despite a strong NIR fluorescence signal was observed in the liver after 2 h injection, the tumor site of TCAD@Ce6 NP treated mice exerted a higher NIR fluorescence than free Ce6 treated ones. As the time goes on, the accumulation of fluorescence signals was gradually reduced in the liver while it gradually increased in the tumor. The fluorescence intensity signals of tumors reached a maximum at 12 h post-injection and with a slight decrease after 24 h injection, suggesting that the TCAD@Ce6 NPs were not subject to rapid metabolism from mice and were excellently *in vivo* tumor-specific by the EPR effect. Furthermore, the mean fluorescence intensity of tumors treated with TCAD@Ce6 NPs and free Ce6 was quantified (Fig. 5B). The fluorescence accumulation in the tumors of Ce6 in TCAD@Ce6 NPs was about 18 fold higher than free Ce6, 12 h post-injection.

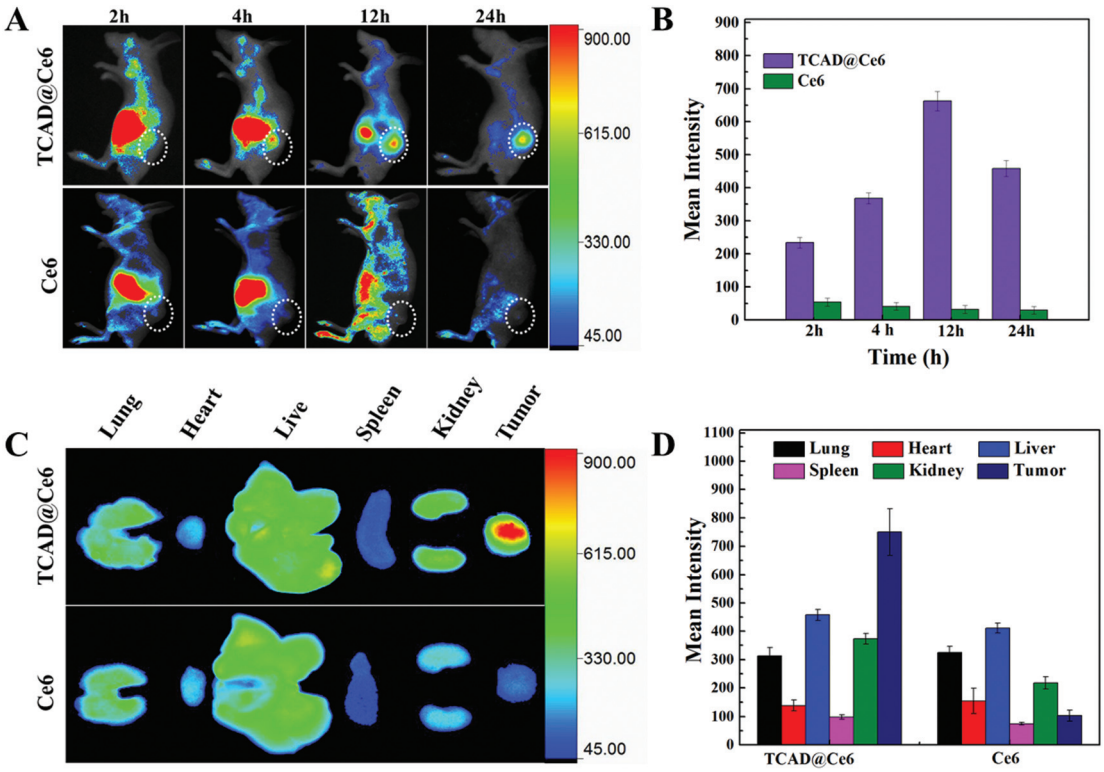

Fig. 5 *In vivo* fluorescence imaging and biodistribution of Ce6 and TCAD@Ce6 NPs. (A) *In vivo* time-dependent whole body fluorescence imaging of A549 tumor-bearing mice after intravenous injection of free Ce6 or TCAD@Ce6 NPs; (B) quantification of average fluorescence signals in the tumor site of (A). (C) *In vitro* fluorescence images of major organs and tumors of mice after intravenous injection of free Ce6 or TCAD@Ce6 NPs over a period of 24 h; (D) quantification of average fluorescence signals of (C). The data are shown as mean ± SD (n = 3).

In addition, *in vitro* fluorescence images of organs (heart, liver, spleen, lung, and kidney) excised from mice (sacrificed at 24 h post-injection) were obtained to intuitively observe the tumor targeting efficacy and tissue distribution of free Ce6 and TCAD@Ce6 NPs. Predictably, similar to the *in vivo* images, TCAD@Ce6 NPs were much more inclined to accumulate to tumors than to stay in normal organs, indicating that they may possess high therapeutic efficiency and low side effects for PDT (Fig. 5C). Nevertheless, the fluorescence of free Ce6 mainly remained in the liver. Similar to free DOX, the TCAD@Ce6 NPs were mainly captured and metabolized by the liver and kidney, resulting in strong fluorescence signals of TCAD@Ce6 NPs in the liver and kidney.[4] The mean fluorescence intensity of organs and tumors was also quantified (Fig. 5D).

Photodynamic therapeutic efficacy of TCAD@Ce6 NPs in tumor-bearing mice

To evaluate the chemo–photodynamic therapeutic efficacy of TCAD@Ce6 NPs *in vivo*, phosphate buffer solution (PBS), free DOX, TCAD NPs, free Ce6 and TCAD@Ce6 NPs were intravenously injected into A549 tumor-bearing mice when the tumor size grew to 90–100 mm^3. To monitor the photodynamic therapeutic efficacy, the tumor sites of free Ce6 and TCAD@Ce6 NP treated mice were irradiated with a NIR laser (633 nm, 50 mW cm^{-2}) for 30 min, after 12 h injection. As shown in Fig. S9,† at 4 days post-irradiation, TCAD@Ce6 NPs plus laser treated mice showed slight hemorrhagic injury at the irradiation tumor site, while the free Ce6/laser or PBS/laser treated group has no noticeable phototoxicity damage. After 14 days, normal tissue had already regenerated at the necrotic scar site of tumors. The change of the tumor volume and body weight of tumor-bearing mice was monitored every 3 days within 18 days. As shown in Fig. 6A, NIR laser irradiation may not significantly inhibit the A549 tumor growth, when A549 tumor-bearing mice were treated with saline. Because of the short blood circulation time and less tumor accumulation of free Ce6, the growth of the tumor tissue of free Ce6 treated mice was not successfully suppressed. Importantly, the tumor was repressed by the singlet oxygen generated by TCAD@Ce6 NPs upon irradiation that is not present in TCAD NPs. It must be acknowledged that the combined TCAD@Ce6/laser treatment was remarkably more efficient in suppressing tumor growth than treatment with free Ce6/laser or TCAD NPs. Unlike free Ce6 or TCAD NPs alone, this observation may be caused by the long retention time and tumor targeting efficacy of TCAD@Ce6 NPs, where the tumor was inhibited by the combination of chemo and photodynamic therapy effects. Moreover, the tumor inhibition efficacy of TCAD NPs and free DOX was significantly different, which may be attributed to the

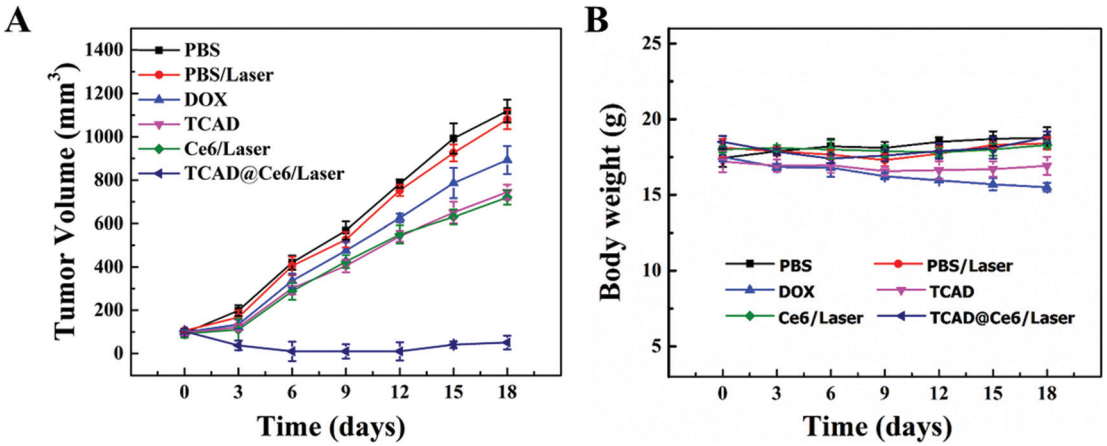

Fig. 6 *In vivo* chemo–photodynamic therapy of TCAD@Ce6 NPs. Tumor volume growth curves (A) and body weight evolution curves (B) of the mice after treatment with free DOX, TCAD NPs, free Ce6/laser irradiation or TCAD@Ce6 NPs/laser irradiation. Data were showed as a mean ± SD (n = 3).

efficient tumor accumulation of acid-sensitive TCAD by the EPR effect and quick excretion by glomerular filtration of free DOX.[5] Interestingly, TCAD@Ce6 NPs with laser irradiation, with an efficient combination of Ce6-mediated phototoxicity and DOX-mediated chemotherapy, led to effective inhibition of tumor growth with the average tumor volume of 95.29% smaller than that of the saline control mice 18 days post-irradiation. All the results confirm the superiority of the chemo–photodynamic combined therapy of TCAD@Ce6 NPs. As we all know, the body weight of the mouse can indicate the treatment-induced toxicity. As shown in Fig. 6B, the body weight loss of mice treated with TCAD NPs was relatively slight compared to those treated with free DOX which had an obvious weight loss. This revealed that the TCAD NPs are a relatively safe prodrug for tumor therapy. Meanwhile, no significant variation of body weight was observed after treatment, indicating that the chemo–photodynamic therapy of TCAD@Ce6 NPs may hardly induce treatment toxicity. Moreover, haematoxylin and eosin (H&E) staining of organs was executed for histopathological examination. As expected, the TCAD@Ce6 NP groups showed neither obvious pathological abnormality or lesion in the heart, spleen, and kidney nor obvious liver damage (Fig. S10†). Overall, the combination treatment of TCAD@Ce6 NPs upon laser irradiation demonstrated remarkable anticancer efficacy with little side effects.

Conclusions

In summary, we successfully prepared novel well-defined acid-sensitive TCAD@Ce6 NPs by a self-assembly process for tumor NIR imaging and chemo–photodynamic combination therapy. The TCAD@Ce6 NPs exhibited stability in water and could be easily hydrolyzed in the acidic microenvironment of tumors. Compared with free Ce6 and DOX, it could significantly enhance the cellular uptake of DOX and Ce6 and induce higher phototoxicity upon NIR laser irradiation. Based on the EPR effect, TCAD@Ce6 NPs could accumulate in tumor sites effectively for tumor NIR fluorescence imaging and efficient inhibition of the growth of A549 tumors under laser irradiation *in vivo*. High performance TCAD@Ce6 NPs can serve as prodrugs for DOX delivery and specific combined chemo–photodynamic therapy, and exhibit great potential in applications such as tumor NIR fluorescence imaging and simultaneous combined chemo–photodynamic therapy in the near future.

Acknowledgements

This work was supported by the National Key Basic Research Program (973 Project) (Project no. 2015CB931802), the National Natural Scientific Foundation of China (grant no. 81225010, 81028009, and 31170961), the 863 project of China (Project no. 2012AA022703 and 2014AA020700), and Shanghai Science and Technology Fund (13NM1401500).

Notes and references

1 M. Chidambaram, R. Manavalan and K. Kathiresan, *J. Pharm. Pharm. Sci.*, 2011, **14**, 67–77.
2 R. H. Blum and S. K. Carter, *Ann. Intern. Med.*, 1974, **80**, 249–259.
3 C. Du, D. Deng, L. Shan, S. Wan, J. Cao, J. Tian, S. Achilefu and Y. Gu, *Biomaterials*, 2013, **34**, 3087–3097.
4 D. Sun, J. Ding, C. Xiao, J. Chen, X. Zhuang and X. Chen, *ACS Appl. Mater. Interfaces*, 2014, **6**, 21202–21214.
5 J. Ding, W. Xu, Y. Zhang, D. Sun, C. Xiao, D. Liu, X. Zhu and X. Chen, *J. Controlled Release*, 2013, **172**, 444–455.
6 O. A. Al-Shabanah, H. A. El-Kashef, O. A. Badary, A. M. Al-Bekairi and M. M. Elmazar, *Pharmacol. Res.*, 2000, **41**, 31–37.

7 N. Duhem, F. Danhier, V. Pourcelle, J.-M. Schumers, O. Bertrand, C. c. S. LeDuff, S. Hoeppener, U. S. Schubert, J.-F. o. Gohy and J. Marchand-Brynaert, *Bioconjugate Chem.*, 2013, **25**, 72–81.
8 L. Pan, Q. He, J. Liu, Y. Chen, M. Ma, L. Zhang and J. Shi, *J. Am. Chem. Soc.*, 2012, **134**, 5722–5725.
9 M. Zheng, C. Yue, Y. Ma, P. Gong, P. Zhao, C. Zheng, Z. Sheng, P. Zhang, Z. Wang and L. Cai, *ACS Nano*, 2013, **7**, 2056–2067.
10 L. Zhang, S. Zhu, L. Qian, Y. Pei, Y. Qiu and Y. Jiang, *Eur. J. Pharm. Biopharm.*, 2011, **79**, 232–240.
11 C.-M. J. Hu and L. Zhang, *Biochem. Pharmacol.*, 2012, **83**, 1104–1111.
12 A. R. Afshar, R. D. Patel and R. D. Jager, *Invest. Ophthalmol. Visual Sci.*, 2012, **53**, 400–400.
13 A. Jhaveri, P. Deshpande and V. Torchilin, *J. Controlled Release*, 2014, **190**, 352–370.
14 Z. Wang, R. Ma, L. Yan, X. Chen and G. Zhu, *Chem. Commun.*, 2015, **51**, 11587–11590.
15 S. Wang, A. Riedinger, H. Li, C. Fu, H. Liu, L. Li, T. Liu, L. Tan, M. J. Barthel and G. Pugliese, *ACS Nano*, 2015, **9**, 1788–1800.
16 W. W. L. Chin, P. W. S. Heng, P. S. P. Thong, R. Bhuvaneswari, W. Hirt, S. Kuenzel, K. C. Soo and M. Olivo, *Eur. J. Pharm. Biopharm.*, 2008, **69**, 1083–1093.
17 R. Bonnett, *Chem. Soc. Rev.*, 1995, **24**, 19–33.
18 Z. Zhao, S. Shi, Y. Huang, S. Tang and X. Chen, *ACS Appl. Mater. Interfaces*, 2014, **6**, 8878–8885.
19 P. Liu, C. Yue, Z. Sheng, G. Gao, M. Li, H. Yi, C. Zheng, B. Wang and L. Cai, *Polym. Chem.*, 2014, **5**, 874–881.
20 C. Zhang, C. Li, Y. Liu, J. Zhang, C. Bao, S. Liang, Q. Wang, Y. Yang, H. Fu and K. Wang, *Adv. Funct. Mater.*, 2015, **25**, 1314–1325.
21 H. Isakau, M. Parkhats, V. Knyukshto, B. Dzhagarov, E. Petrov and P. Petrov, *J. Photochem. Photobiol., B*, 2008, **92**, 165–174.
22 Y. Li, Y. Yu, L. Kang and Y. Lu, *Int. J. Clin. Exp. Med.*, 2014, **7**, 4867.
23 H. Y. Yoon, H. Koo, K. Y. Choi, S. J. Lee, K. Kim, I. C. Kwon, J. F. Leary, K. Park, S. H. Yuk and J. H. Park, *Biomaterials*, 2012, **33**, 3980–3989.
24 A. Yuan, B. Laing, Y. Hu and X. Ming, *Chem. Commun.*, 2015, **51**, 6678–6680.
25 V. Karabanovas, A. Skripka, J. Valanciunaite, R. Kubiliute, V. Poderys and R. Rotomskis, *J. Nanopart. Res.*, 2014, **16**, 1–8.
26 J.-H. Park, Y.-H. Moon, I.-S. Bang, Y.-C. Kim, S.-A. Kim, S.-G. Ahn and J.-H. Yoon, *Lasers Med. Sci.*, 2010, **25**, 705–710.
27 J. R. Fischer, K. R. Harkin and L. Freeman, *Vet. Ther.: Res. Appl. Vet. Med.*, 2001, **3**, 465–473.
28 N. Cao and S.-S. Feng, *Biomaterials*, 2008, **29**, 3856–3865.
29 M. Sadoqi, C. Lau-Cam and S. Wu, *J. Colloid Interface Sci.*, 2009, **333**, 585–589.
30 H.-J. Youk, E. Lee, M.-K. Choi, Y.-J. Lee, J. H. Chung, S.-H. Kim, C.-H. Lee and S.-J. Lim, *J. Controlled Release*, 2005, **107**, 43–52.
31 G. Tian, X. Zheng, X. Zhang, W. Yin, J. Yu, D. Wang, Z. Zhang, X. Yang, Z. Gu and Y. Zhao, *Biomaterials*, 2015, **40**, 107–116.
32 Y. Mi, J. Zhao and S.-S. Feng, *J. Controlled Release*, 2013, **169**, 185–192.
33 L. Milane, S. Ganesh, S. Shah, Z.-f. Duan and M. Amiji, *J. Controlled Release*, 2011, **155**, 237–247.
34 F.-Q. Hu, L.-N. Liu, Y.-Z. Du and H. Yuan, *Biomaterials*, 2009, **30**, 6955–6963.
35 G. Tian, W. Ren, L. Yan, S. Jian, Z. Gu, L. Zhou, S. Jin, W. Yin, S. Li and Y. Zhao, *Small*, 2013, **9**, 1929–1938.
36 M. S. Muthu, D. T. Leong, L. Mei and S.-S. Feng, *Theranostics*, 2014, **4**, 660.
37 R. Rotomskis, J. Valanciunaite, A. Skripka, S. Steponkiene, G. Spogis, S. Bagdonas and G. Streckyte, *Lith. J. Phys.*, 2013, 53.
38 S. Mitra, U. Gaur, P. Ghosh and A. Maitra, *J. Controlled Release*, 2001, **74**, 317–323.
39 Z. Gao, A. N. Lukyanov, A. Singhal and V. P. Torchilin, *Nano Lett.*, 2002, **2**, 979–982.
40 G. Kwon, M. Naito, M. Yokoyama, T. Okano, Y. Sakurai and K. Kataoka, *Langmuir*, 1993, **9**, 945–949.
41 P. Huang, D. Wang, Y. Su, W. Huang, Y. Zhou, D. Cui, X. Zhu and D. Yan, *J. Am. Chem. Soc.*, 2014, **136**, 11748–11756.
42 H. S. Han, J. Lee, H. R. Kim, S. Y. Chae, M. Kim, G. Saravanakumar, H. Y. Yoon, D. G. You, H. Ko and K. Kim, *J. Controlled Release*, 2013, **168**, 105–114.
43 H. Wang, F. Xu, Y. Wang, X. Liu, Q. Jin and J. Ji, *Polym. Chem.*, 2013, **4**, 3012–3019.
44 M. Li, Z. Tang, S. Lv, W. Song, H. Hong, X. Jing, Y. Zhang and X. Chen, *Biomaterials*, 2014, **35**, 3851–3864.
45 M. Yoshida, I. Shiojima, H. Ikeda and I. Komuro, *J. Mol. Cell. Cardiol.*, 2009, **47**, 698–705.
46 H. Jeong, M. Huh, S. J. Lee, H. Koo, I. C. Kwon, S. Y. Jeong and K. Kim, *Theranostics*, 2011, **1**, 230.
47 Y.-Z. Zhao, C.-Z. Sun, C.-T. Lu, D.-D. Dai, H.-F. Lv, Y. Wu, C.-W. Wan, L.-J. Chen, M. Lin and X.-K. Li, *Cancer Lett.*, 2011, **311**, 187–194.

